Scientific Research Publishing

International Journal of Geosciences, 2016, 7, 1122-1143
http://www.scirp.org/journal/ijg
ISSN Online: 2156-8367
ISSN Print: 2156-8359

Determination of the Structural Lineaments in the Kribi-Campo-Ma'an Area from a Multi-Scale Analysis of Gravity Data Using the HGM and Euler 3D Deconvolution Approaches

Owona Angue Marie Louise Clotilde[1,2*], Assembe Stephane Patrick[2,3], Njingti Nfor[1], Ngoh Jean Daniel[2], Ndougsa Mbarga Theophile[1,2*], Kue Petou Rokis[2], Bisso Dieudonné[2]

[1]Department of Physics, Advanced Teacher Training College, University of Yaoundé I, Yaoundé, Cameroon
[2]Postgraduate School of Sciences, Technologies & Geosciences, University of Yaoundé I, Yaoundé, Cameroon
[3]Department of Physics, Faculty of Science, University of Bamenda, Bambili, Cameroon
Email: *mlasseowona@yahoo.fr, *tndougsa@yahoo.fr

How to cite this paper: Clotilde, O.A.M.L., Patrick, A.S., Nfor, N., Daniel, N.J., Theophile, N.M., Rokis, K.P. and Dieudonné, B. (2016) Determination of the Structural Lineaments in the Kribi-Campo-Ma'an Area from a Multi-Scale Analysis of Gravity Data Using the HGM and Euler 3D Deconvolution Approaches. *International Journal of Geosciences*, **7**, 1122-1143.
http://dx.doi.org/10.4236/ijg.2016.79085

Received: May 6, 2016
Accepted: September 27, 2016
Published: September 30, 2016

Abstract

With the aim to produce a detailed structural map and then enhance the geological information of the south-western Cameroon, a field gravity study is carried out in the Kribi-Campo-Ma'an area (SW Cameroon). This study area is assumed to undergo pending active tectonics as witnessed by several earthquakes [1]. Besides, the area has been affected by some shears that gave rise to many major faults including the Kribi-Campo Fault (KCF). This N-S lineament is an active fault corresponding to the NW margin of the CC [2] [3] and related to the development of the Kribi-Campo basin. The gravity data analysis enables to highlight many deeply- seated structural features trending in the NE, NNE, N-S, NNW, NW and E-W directions in this region. The NW-SE trend is more strongly developed than the other identified trends and could have deeply affected the major NNE structure. The NNE-SSW to N-S fractures and faults which are local relays of the Kribi-Campo fault are related to the Kribi shear zone. The fairly good clustering observed on local maxima of the horizontal gradient magnitude enables to suggest that the contacts outlined have vertical to subvertical dips. However, a probable interpretation of these features is that they are vertical to subvertical faults which follow the aforementioned directions. The location of the study area in the gulf of Guinea suggests that it sustains tectonics related both to the equatorial and the south Atlantic oceans opening.

Keywords

Gravity Anomaly, Lineament, Kribi-Campo Fault, Dip

1. Introduction

The current study investigates the transition zone between the NW margin of the Congo Craton (CC) and the North Equatorial Fold Belt (NEFB). Indeed, though the CC formations dominate the area, many authors [4]-[6] additionally invoke the thrusting of the NEFB over the CC which was confirmed by [2]. The area is assumed to undergo pending active tectonics as witnessed by several earthquakes [1]. Besides, the study area has been affected by some shears that gave rise to many major faults including the Kribi-Campo Fault (KCF). This N-S lineament is an active fault corresponding to the NW margin of the CC [2] [3] and related to the development of the Kribi-Campo basin. All these results correlate with the regional scale geology, although some miscellaneous obscuring points remain and should be checked.

With the aim to produce a detailed structural map of the area, a ground gravity study is carried out in the Kribi-Campo-Ma'an area (SW Cameroon). The interpretation of gravity data is one of the most efficient methods to detect buried features, for it indicates some important structural features that will not be able to follow through using morphotectonical tools. Linear anomalies are important in the interpretation of gravity data, because they indicate some important structural features and contacts. We focus the interpretations on the strong contrasts (gradients) exhibited by the Bouguer anomaly map, in order to infer zone of discontinuities such as faults, dykes and flexures. For the present study, two combined methods are used, they are both useful in simplifying and focusing on the complex pattern of anomalies over their source. This consists in a prior interpretation of the Bouguer map followed by an analysis based on the horizontal gradient coupled with the upward continuation methods. The combination of horizontal gradient coupled with upward continuation revealed consistency in detailed studies and led to the delineation of major geological structures and tectonic lineaments [1]. These serve as edge-detector and geometrical analysis tools. Many previous geophysical studies [1] [2] [7]-[12] provide useful geological knowledge information, but the detailed geological information of region is still to be improved. The purpose of this work is to use a multi-scale analysis of gravity data to enhance the previous results and give a precise lineament mapping in the Kribi-Campo region.

2. Geological Setting

The study area is located in SW-Cameroon between latitudes 2˚00'N - 3˚00'N and longitudes 9˚45'E - 10˚45'E (**Figure 1**). The area is totally underlained by the Ntem Complex formations and occurrence of Panafrican terrains evolving at the NW margin of the Congo Craton. The Paleoproterozoic elements are represented by the Nyong Unit [1] [6]. The Archaean formations that constitute the basement are mostly charnockites,

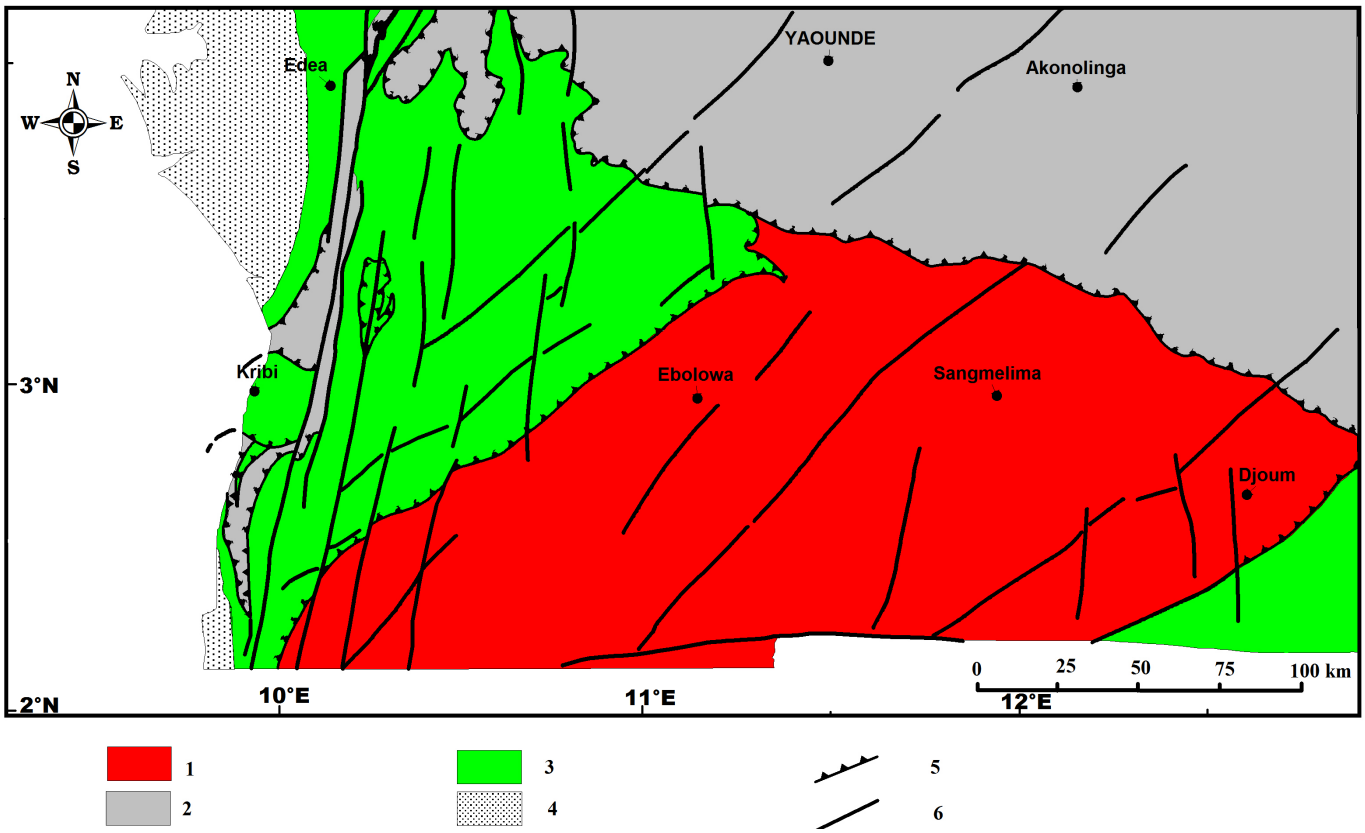

Figure 1. Simplified geological map of the SW-Cameroon [6] [19]. 1: Archaen Basement; 2: Neoproterozoic cover; 3: Neoarchaen-paleoproterozoic cover; 4: Post Panafrican cover; 5: Thrust fault; 6: fault.

greenstones belt rocks and potassicgranitoids [2] [7] [13].

The previous studies have revealed that the area mainly underwent brittle deformations related to multistage compressional and extensional tectonics that give rise to major faults. These are mainly characterised by the Kribi-Campo Fault (KCF) system which is herein defined as a continuation of the Sanaga Fault [1]-[3] [14] [15]. Other studies [16] [17] supported by [18] also link the KCF to an offshore fault system known as the Kribi Fracture Zone inferred as the eastern end of the Ascension Fracture Zone settled during the W Gondwana break-up.

The gravimetric modelling along a SW-NE profile passing through Kribi and Lolordorf shows that the thickness of the upper crust is approximately equal to 18 km [2] [8]. [2] presented a 2D model of resistivity according to a profile which begins substantially at the end of the SW negative gravity anomaly contours of Bipindi and covers 3/4 of the anomaly zone in the direction of the NE-SW elongation. This 2D resistivity model has two resistant blocks separated by the less resistant rocks. The approximate location depth of roofs and bases of both resistant blocks was 1 km and 14 km, respectively. Upward from the base, the right end of the western block dips SW while the left end of east block dips the SE, indicating in each case, a gradual uplift from 14 km to about 8 km depth [2].

3. Materials and Methods

3.1. Gravity Data

The dataset used for the current study is a combination of recent and historical data. The recent data have been collected in March 2015, using a Lacoste & Romberg G-823 gravimeter. The historical data come from 183 gravity stations that are part of the dataset collected by ORSTOM in 1967. The recent dataset corresponds to additional 223 gravity stations realised in the Kribi-Campo-Ma'an region (which until this gravity campaign done, was not covered by ground geophysical studies). This led to a resulting dataset of 406 gravity measurement sites.

The recent geophysical campaign involves two collecting data profiles, along the N-S and W-E direction as well. The N-S survey profile follows the coastal Kribi-Campo road while the W-E (perpendicular to the first) was realised from Campo to Ma'an, passing through the Memve'ele hydro-electrical dam site. The distance between different stations ranges from 0.5 to 2 km (black circles on Figure 2). The base station was

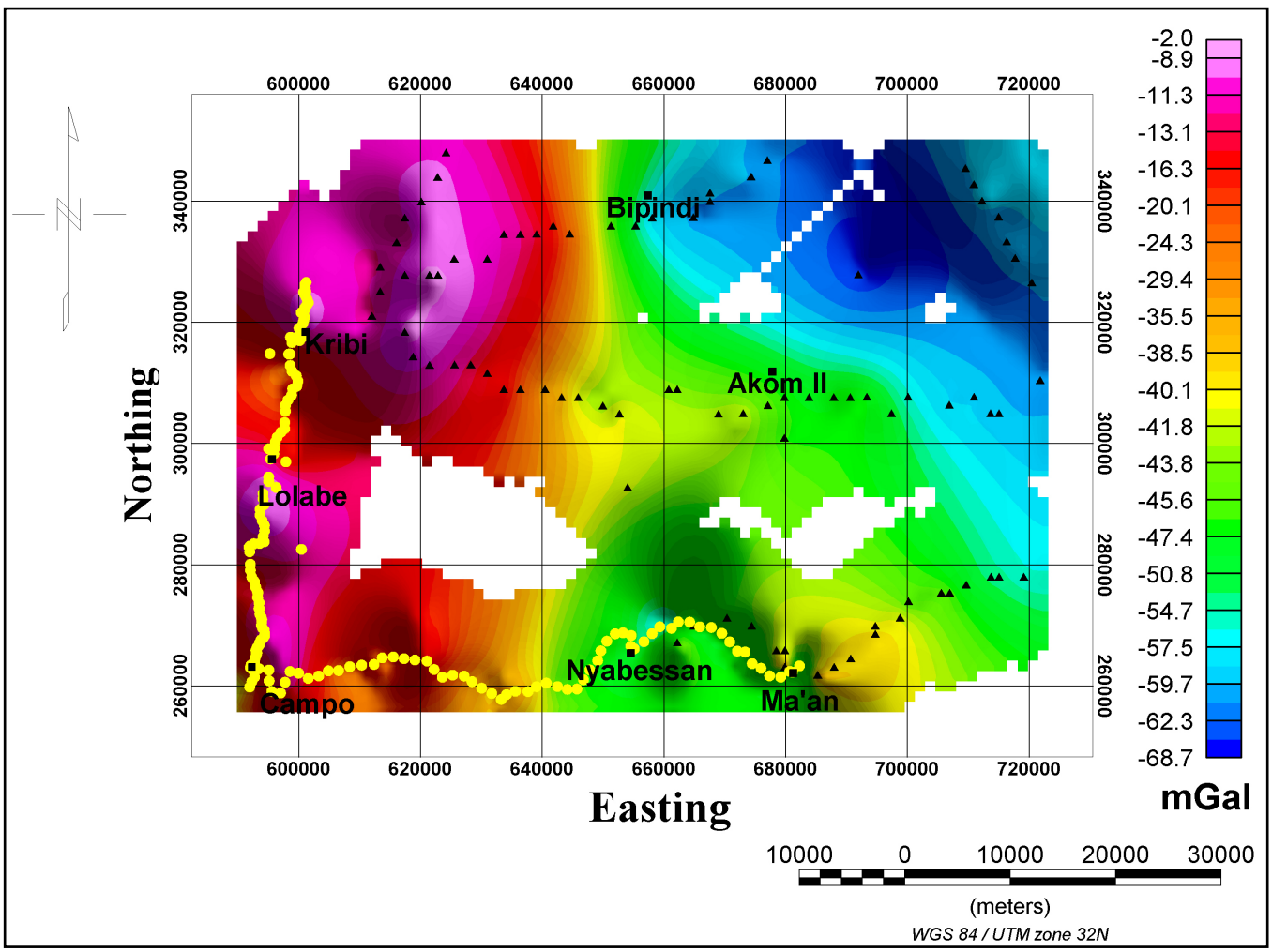

Figure 2. Bouguer gravity anomalies map of the study area with distribution of the measurements stations. Yellow circles represent the recent dataset and black triangles, come from the Orstom's dataset.

set at Kribi, as for past gravity campaigns [20] [21], in order to increase the accuracy of these new collected data and also, because the Kribi base station is linked to the international base station of Douala. The irregularities in the distribution of the gravity points are due to the difficulties in accessing the area, which belongs to the tropical rain forest. Before merging data, the recent measurements were corrected from the luni-solar tidal effects and instrumental drift (herein assumed to be linear in time). Free-air and Bouguer reductions based on a mean density of 2.67 g/cm^3 were applied and the simple Bouguer anomalies have been derived. The resulted Bouguer anomalies are the basic data used in this study context (**Figure 2**). Since data was collected onshore, the sea-data have not been included in this study.

The simple Bouguer anomaly map (**Figure 2**) of the region is obtained after interpolation by combining the existing data set and the one collected during the 2015 campaign, and then applying a minimum curvature gridding algorithm implemented in Oasis Montaj 8.0 software. The Bouguer anomaly values in the grid are encompassed in the −68.7 mGal −2.0 mGal interval.

3.2. Methodology

This study applies the horizontal gradient technique to upward-continued gravity grids at various heights, in order to assess the peaks in the concerned grids. The technique is referred to as the multiscale analysis [9] [22]. It appears straight forward that the base analytical tools are the Upward Continuation (*UC*) and the Horizontal Gradient (HG) methods. In addition, we performed the 3-D Euler Deconvolution in an attempt to find depth to basement of investigated lineaments.

3.2.1. The Upward Continuation (UC)

It is shown that to investigate large geologic features in the region, gravity data were generally upward continued to nominal elevations [23]-[25]. The upward continuation (*UC*) consists in recalculating a potential field measured on a given observation plane at a given height to an observation plane at a different height [26] [27]. The equation in the wave number domain filter to produce *UC* is simply:

$$UC = e^{-h\omega} \tag{1}$$

where h is the continuation height and ω is radial frequency.

This function decays steadily with increasing wave number, attenuating the higher wave numbers more severely, thus producing a map in which regional features predominate [1] [9] [27] [28].

3.2.2. The Horizontal Gradient Magnitude (*HGM*)

The horizontal gradient is an operation that measures the rate of change of a potential field in the x and y directions [29] in order to image subsurface structures. However, the total horizontal gradient magnitude (*HGM*) is preferred. *HGM* operator is defined by the relation below:

$$HGM\left(x,y\right) = \sqrt{\left(\frac{\partial G}{\partial x}\right)^2 + \left(\frac{\partial G}{\partial y}\right)^2} \tag{2}$$

where G is the Bouguer gravity field.

The horizontal gradient method was used to locate the boundaries of density contrast from gravity data [29] [30]. These results mark the top edges of gravity or density boundaries. Thus, the maximum value of the horizontal gradient anomalies is placed on top of the sources edges. However, offsets occur when edges are not vertical or when several anomalies are close together. The biggest advantage of the horizontal gradient method is its low sensitivity to the noise in the data, because it only requires calculations of the two first-order horizontal derivatives (x- and y-directions) of the gravity field [31]-[33].

Once the Bouguer grid is upward-continued at a given height, the HGM filter is applied to the resulting grid then local peaks are extracted. The extraction of local peaks (maxima) is performed using [33] approach. The upward continuation processing of the Bouguer gravity map at various altitudes, followed by horizontal gradient maxima computation for each level yielded these maxima. The progressive migration while increasing upward continuation height indicates the dip of features outlined [1] [9] [34]. The technique, referred to as the multi-scale horizontal derivative (MSHD) analysis, has been applied to upward-continued Bouguer map of the Kribi-Campo area at five heights: 2, 4, 6, 8 and 10 kilometres.

3.2.3. 3-D Euler Deconvolution Method

The application of Euler Deconvolution acknowledged many significant advances since its introduction in geophysics, as interpretation tool for potential field data by [35]. In the current study, the 3-D Euler Deconvolution tool was used in an attempt to find depth to basement of investigated lineaments. This technique provides automatic estimates of source depth-location. Indeed, the 3-D Euler Deconvolution creates a solution set from grid dataset containing proposed sources which "explain" the grid's anomalies. It calculates location, depth below sensor and reliability for each solution as well as error estimated in the form of standard deviations. Therefore, 3-D Euler Deconvolution is both a boundary finder and depth estimator [35] [36].

The original 2D method was adapted for use, as a grid-based method by [36] based on the Euler's homogeneity Equation (3):

$$\left(x-x_0\right)\frac{\partial M}{\partial x}+\left(y-y_0\right)\frac{\partial M}{\partial y}+\left(z-z_0\right)\frac{\partial M}{\partial z}=N\left(B-M\right) \tag{3}$$

where B is the regional value of the gravity field and (x_0, y_0, z_0) is the position of the causative source which produces the field M measured at (x, y, z). N is so called structural index. For each position of the moving window, an over-estimated system of linear equations is solved for the position and depth of the sources [35]-[37].

The most critical parameter in the Euler Deconvolution is the structural index, N [35]. This is a homogeneity factor relating the potential field and its gradient components to the location of the source. Essentially, N measures the rate of change of the fields with distance from the source (fall-off-rate) and is directly related to the source dimensions. Therefore, by changing N, we can estimate the geometry and depth of the

gravity sources. A poor choice of the structural index has been shown to cause a diffuse solution of source locations and serious biases in depth estimation. Both Thompson [35] and Reid *et al*. [36] [37] suggested that a correct N gives the tightest clustering of the Euler solutions around the geologic structure of interest. For gravity data, physically plausible N values range from 0 to 2.

On the same previous Bouguer grid, the 3-D Euler Deconvolution is applied for a given structural index N to automatic estimate of source depth-location. The results comparison of this MSHD and 3-D Euler of the Bouguer help to provide a precise lineament map.

4. Results

4.1. Bouguer Gravity Anomalies

Figure 3 below shows the Bouguer anomaly map of the study area. It reflects lateral variations of density in the basement and shows several anomalies with various values and shapes. It is produced from the interpolation of the gravity map from Figure 2

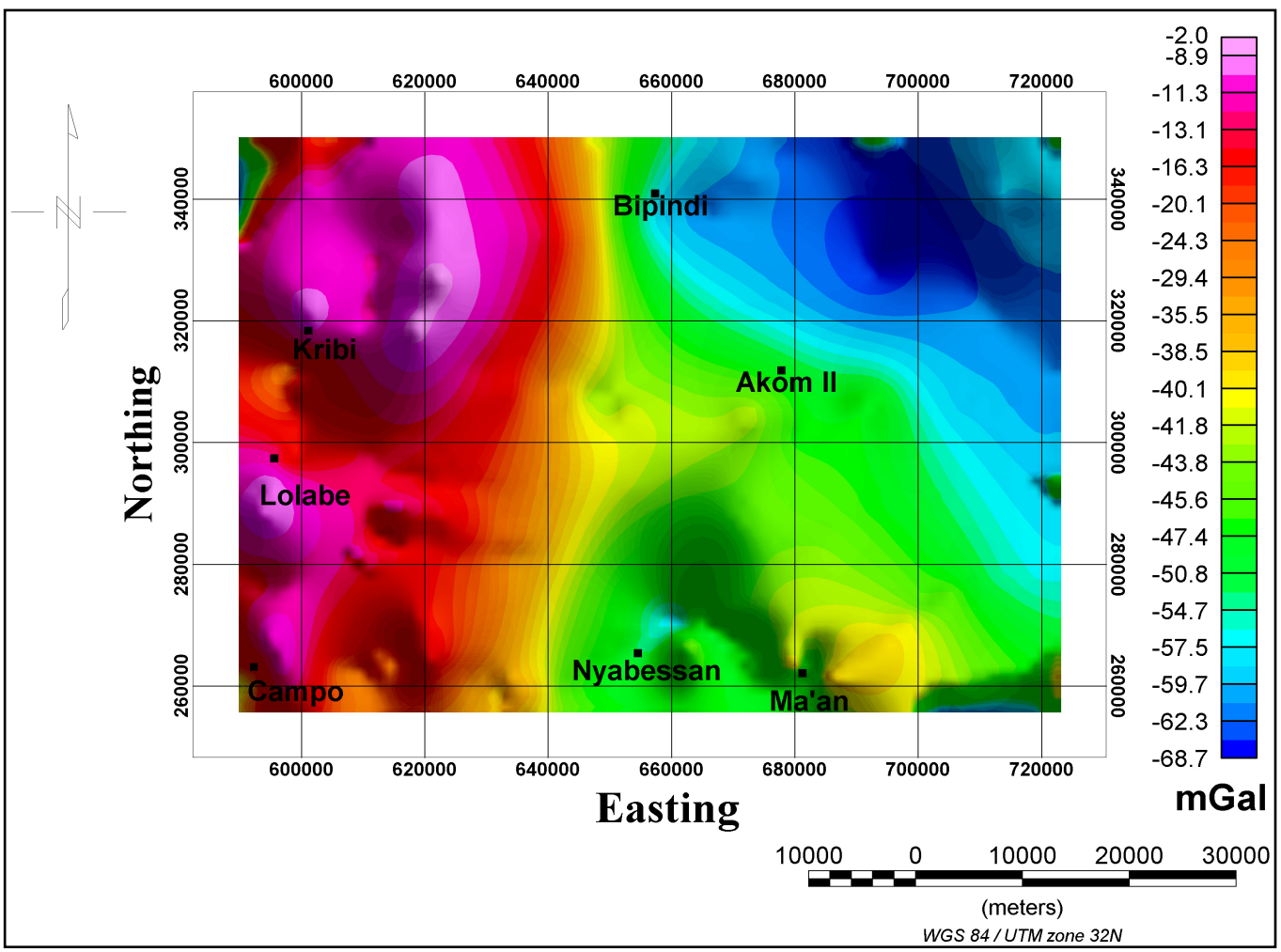

Figure 3. Bouguer gravity anomalies map of the study area. The map results from the interpolation of the map in Figure 2.

which enabled to fill the grid dummies. It is characterized by gravity values ranging from −68.7 mGal to more than −2.0 mGal. This is in accordance with the fact that gravity data have been collected onshore (and by the fact that the continental crust is less dense that the oceanic crust).

The Bouguer map displays three main types of gravity anomalies over the study area. These are accordingly high, intermediate and low values gravity anomalies. High gravity anomalies (values ranging from −38.5 to −2.0 mGal) occupy the broad western side of the study area. The broad zone characterised by high gravity anomaly values also exhibits four peaks. The peaks located near the margin (three peaks) are circular and line up along the N-S direction, from Campo to Kribi. The broadest peak is shifted to the right, east of Kribi; it is oval and nearly curved to the left at its upper part. All these peaks may correspond to dense or basic intrusive bodies within the main formation broadly characterised by the high intensity anomaly values. The anomaly field herein most likely corresponds to the signal of Paleoproterozoic terrains that occur in the study area's part. Alternatively, the two peaks observable in Kribi neighbourhood may rather be considered as a unique very high-valued anomaly corresponding to a ring complex affected by a nearly N-S trending discontinuity. In Addition, a moderate high gravity anomaly occurs at the SE edge of the Bouguer map. This is a NW-SE elongated anomaly that is probably caused by topographic effects or an intrusive body. The high gravity anomaly values domain is flanked to the east by an intermediate anomaly domain whose values are between −50.8 mGal to −38.5 mGal.

The domain characterised by intermediate Bouguer's anomaly values forms the centre domain. This domain is separated from the previous described domain by a N-S trending gravity gradient west from Nyabessan (**Figure 3**). This suggests a discontinuity which seems gradational to south and steep to the north of the study area. Globally, the area is fairly quiet although it is disturbed by a high NW elongated anomalies (−40.1 mGal to −38.5 mGal) at Ma'an and a trough at Nyabessan, respectively. The anomaly peak at Ma'an is affected by a NE discontinuity that can be interpreted as a lineament. Careful observation of the Bouguer gravity map tends to suggest the existence of NE-SW discontinuity between Akom II and Nyabessan. This is probably a shear zone or faulting that affects the deep basement. The gravity anomaly field herein may correspond to the signature of the Archaean basement of the study area. The intermediate gravity anomaly field domain narrows to the north at the vicinity of Bipindi. This domain is separated to the east by a NW-SE trending domain of very low gravity values herein referred to as the NE domain.

The NE domain is characterised by very amplitude anomaly values within the interval −68.7 mGal to −50.8 mGal interval. It is a NW-SE trending domain at the NE margin of the study area, thus implying a NW-SE contact limit with the centre domain to its west flank. The domain forms a NW-SE basin-like environment NE of Akom II. The basement of this basin is made up of low density formations, probably granites or granitoids of the Ntem complex.

The general disposition of anomalies on the Bouguer map from the study area shows

a decrease in the anomaly field values from the west to east. This corresponds to a decrease in density from west to east. We therefore assume that formations to the west are denser than those to the east, as we move from the shore to the hinterland.

4.2. Upward Continuation of Bouguer Gravity Anomalies

The upward continuation of the gravity field at increasing heights highlights the gravity effect of deep sources. This is because upward continuation suppresses the signals due to small, shallow bodies [38].

The map above (**Figure 4**) shows the Bouguer gravity anomalies map upward continued to 10 km from the study area. Although continuations are realised for various heights and used in the subsequent sections, the **Figure 4** (corresponding to the highest level) above has been chosen to illustrate the behaviour of gravity anomaly affecting the basement. Some previous observations made on the simple Bouguer anomalies (**Figure 3**) are confirmed although differences are noticeable on this map. The moderate gravity anomalies observed in the study area map are well smoothed and could reflect the gravity effects of deep or regional structures, while other anomalies are better amplified.

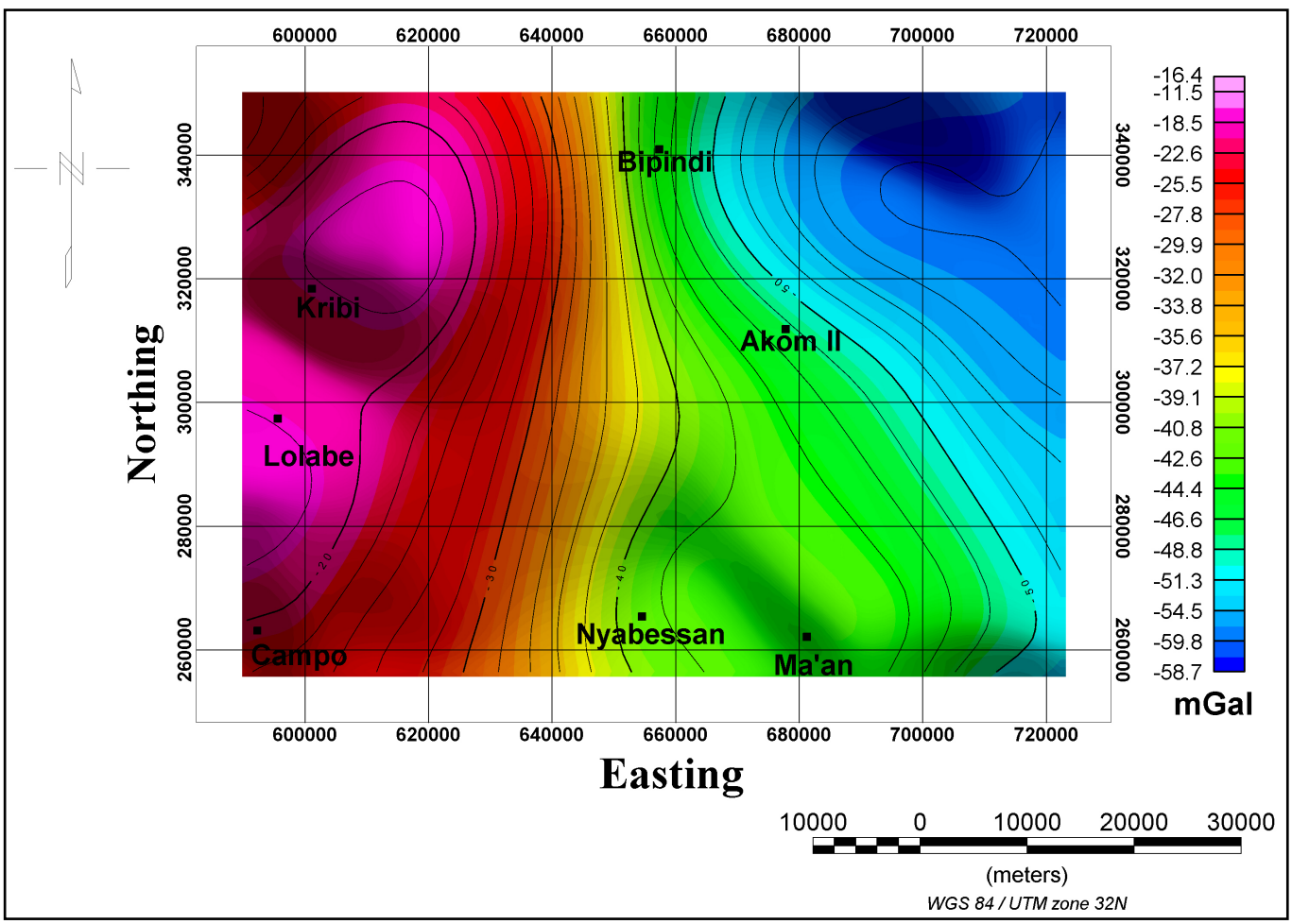

Figure 4. Bouguer gravity anomalies upward continued to 10 km.

This proofs that, they are also regional anomalies probably caused by deep or regional basement structures.

All these gravity anomalies tend to expand as the upward continuation height increases. The heavy anomalies trend broadly N-S. Besides there is a NW trough observed on both maps (Figure 3 and Figure 4) probably caused by faulting processes.

4.3. Horizontal Gradient Magnitude (HGM)

To enhance lateral boundaries of density contrast in potential field data, we calculated the horizontal gradient of the Bouguer gravity anomaly. The horizontal gradient of the Bouguer anomaly data was calculated in the frequency domain and its amplitudes provided the horizontal gradient map presented in Figure 5 below. The horizontal gradient magnitude map obtained enhances some short wavelength features and highlights areas with steep density variations, which could be interpreted either as faults, geologic contacts, or as intrusive formations as well. It is observed that the pattern of the high gradient anomalies is broad, not like sharp ones of ideal vertical boundaries of density contrast.

Analysis of the whole horizontal gradient magnitude map (Figure 5) highlights

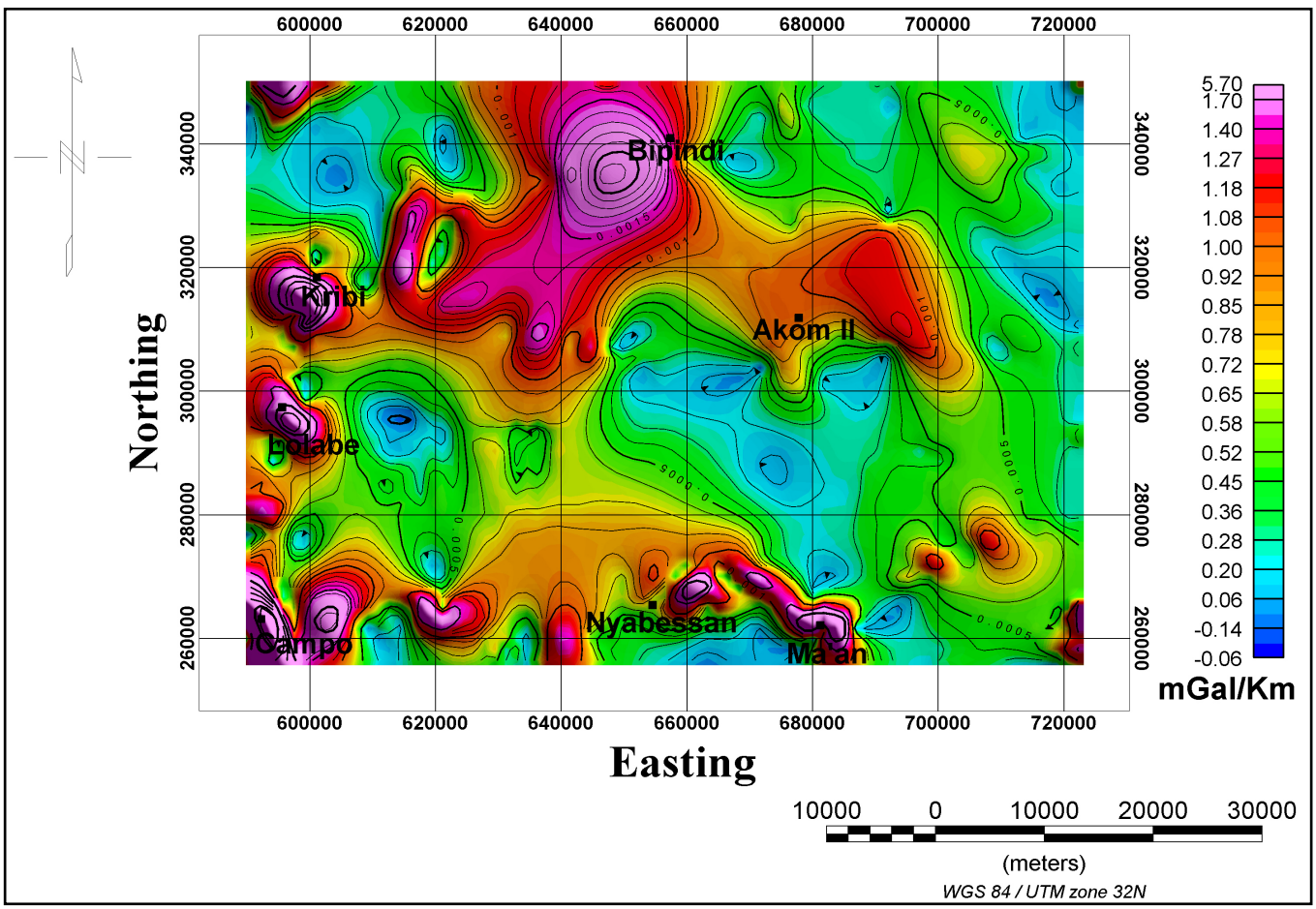

Figure 5. Horizontal gradient magnitude of Bouguer gravity anomalies map of the study area.

various geological features, which are characterized by differences in gradients values. The map exhibits different gradients values zones with various amplitudes, shapes and little coherent regional fabric. These different zones are bounded by relative steep or abrupt gradients in some places. The horizontal gradient values range from 0.2 mGal/km to 5.7 mGal/km. It appears on **Figure 5** that there is a broad region of high horizontal gradient anomalies (magenta to red colour) that dominates the entire map. This region departs from the background gradient anomaly mainly characterised by greenish colours.

The high horizontal gradient anomalies domain is characterized by a relative high gradient value (magenta to red colour) disseminated in the whole map within the moderate background (greenish). This domain is dominantly spans from the west to nearly centre-east part of the study area. The trends of these high amplitude horizontal gradients are approximately NNE, NNW to N-S in certain places. Besides, there are many very low intensity gradient anomalies that are also noticeable on the horizontal gradient magnitude map (**Figure 5**). These anomalies are characterized by troughs (blue colour) that affect the background field. The low amplitude anomalies are majorly closed and elongated along the NW-SE and E-W directions, though other trends are seemingly acknowledgeable.

To sum up, the appearance of the horizontal gravity map (**Figure 5**) suggests that the study area underwent an intense tectonic activity that affected its basement. This tectonic activity is testified by the fault and fracture occurrences which are represented by elongated high gradients; many intrusions represented by close-contoured high amplitudes anomalies. The horizontal gradient map shows that the west to centre of the study area is strongly marked by that brittle tectonics more than the eastern side.

Accordingly with the geological information, in the whole map, the gravity gradient highs, are bounded by relatively steep gradients. The presence of high gravity gradients, which occur over these basic rocks, suggests the existence of a suture zone between two blocks of the crust or the existence of dense mantle rock or uprising of some mantle materials in these places. It might also represent the thinning of upper crust due to the mantle materials uplift. Then, a relative elongated high gravity gradient anomaly at the north-western and middle southern portion could be due to the uplift of deeper mantle materials, dense than the surface materials *i.e.* seems to represent the signature of dense mantle materials or rocks in this zone. This zone with a strong gradient could also corresponding to contact or fault structures.

In addition, the relative low gradient value also highlighted on the horizontal gradient of the Bouguer gravity anomaly, might indicate the presence of lower density materials. It uplifts zones of high and moderate gradients. The long linear gradient anomalies are indicative of intra-basement faults or crustal block edges.

4.4. Edges Detection with the Horizontal Gradient Magnitude Maxima

The maxima of the horizontal gradient of a the Bouguer anomalies shown in **Figure 6** below help to locate contacts associated with abrupt changes in density and the mul-

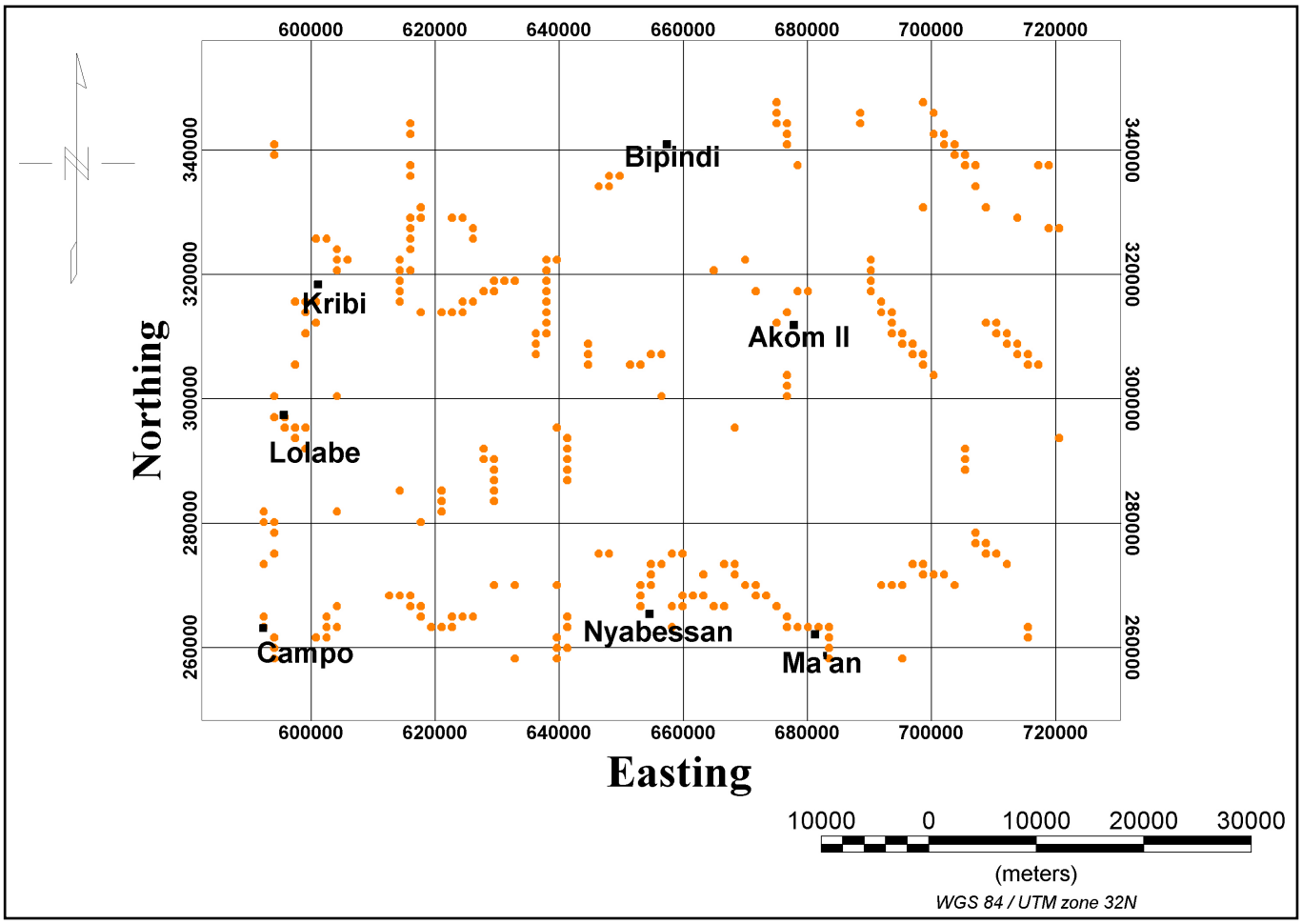

Figure 6. Maxima of the horizontal gradient magnitude of Bouguer gravity anomalies at 0 km.

ti-scale analysis of these maxima involves upward continuation of the gravity field to different heights with a view to characterize the vertical extension of anomalous structures. Faults and contacts are expressed by a quasi-linear disposition of many maxima and horizontal limits of intrusive bodies are showed by their quasi-circular disposition [9] [29] [39]. In general, the local peaks in the magnitude of the horizontal gradient give the locations of the large density contacts. The steepest horizontal gradient of a gravity anomaly will be located directly over the edge of the body if the edge is vertical and far away from any other edge or source [40].

The maxima of the horizontal gradient of the Bouguer anomalies showed in **Figure 6** below exhibit most structures features as faults/fractures and geologic boundaries. The linear local peaks of horizontal gradient magnitude trending in NNW, NNE and N-S directions. While the circular disposition of local peaks of horizontal gradient magnitude occurred at the west side present the southward extension.

Multi-scale edge mapping is a process of edge detection in potential field data. During the process, the positions of gradients maxima are detected across multiple heights of upward continuation. The multi-scale analysis horizontal gradient map is obtained

by showing the maxima from various levels on the same plot. The offsets observed on the arrangement of maxima inform about the dip of the structure outlined [41] [42].

Figure 7 below is the multi-scale edge map from horizontal gradient of upward continued Bouguer anomaly map from 0 to 10 km height respectively (colour description is provided with the map of Figure 6). The analysis of the multi-scale map (Figure 7) below enables to outline many geological features, especially lineaments. According to Figure 8, the map enables to highlight many lineaments. The features outlined correspond probably to the major elements that affect the basement. These are lineaments which follow the E-W, N-S, NE and NW directions. However, the NW directions are the more represented. Some of these lineaments are consistent with the features outlined from the Bouguer anomaly map (Figure 3).

The lineaments highlighted on Figure 7 can be interpreted as contacts or faults, though the interpretation as contacts seems more consistent. The multi-scale analysis shows that most the local maxima plotted are clustered along well designed lines. In

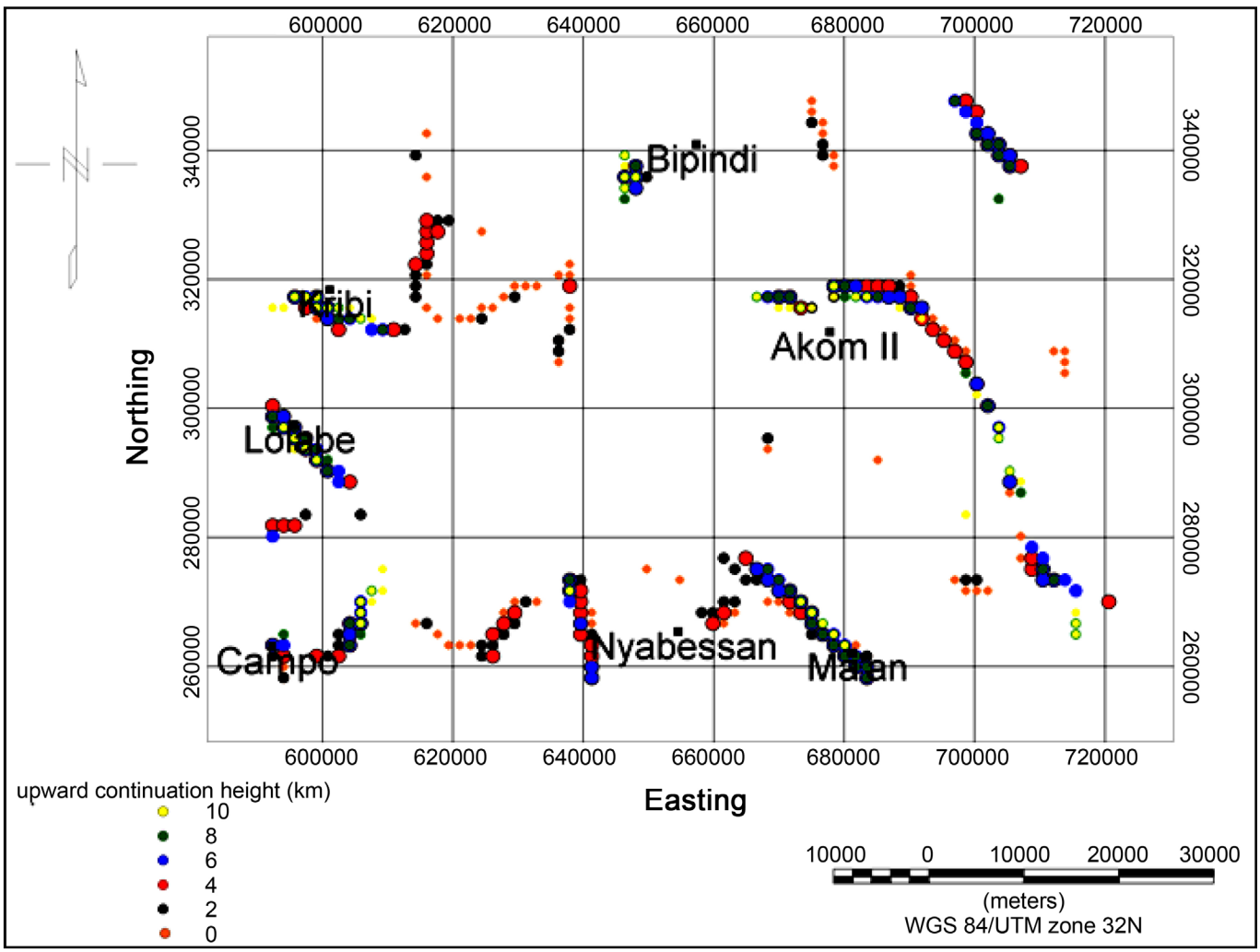

Figure 7. Superposition of the maxima of the horizontal gradient magnitude at various altitudes. Local peaks are represented by proportional colored circles.

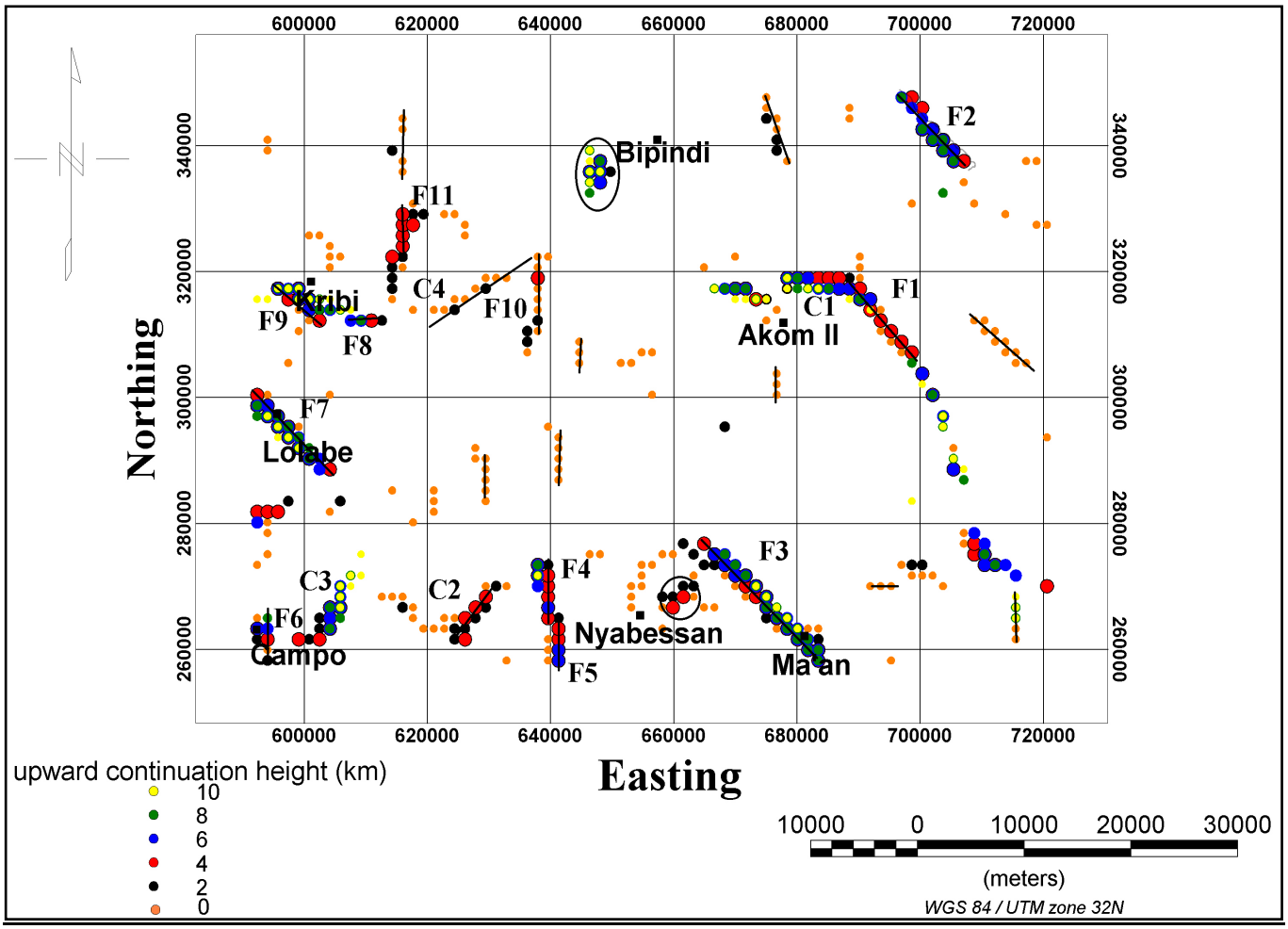

Figure 8. Superposition of the maxima of the horizontal gradient magnitude of Bouguer gravity anomalies upward continued to 0, 2, 4, 6, 8 and 10 km respectively with several designed lineaments.

addition, these maxima don't appear to be much offset from the cluster lines outlined. These allow us to interpret the lineaments as contacts, whose directions are E-W, N-S, NE-SW and NW-SE (the dominant directions being NW-SE and N-S as shown on the map from Figure 7). The good clustering or few offsets observed on local maxima enable to suggest that the contacts outlined have vertical to subvertical dips. However, probable interpretation of these features is that they are vertical to subvertical faults which follow the aforementioned directions.

In Figure 8, there is a major lineament that occurred at the Akom II North-eastern side which could be interpreted as the contact. In the other hand, this major lineament seems to be a buried fault named F1, directed NW-SSE. The same observations are made at Campo (fault F6) and Kribi (F8 and F9 faults) neighbouring. The anomaly at Bipindi could be considered as an intrusion while a major NE-SW deep fault occurs eastern of Kribi.

Close inspection of the features on Figure 8 reveals that, the study area is affected by deep-seated structural lineaments oriented in the NW-SE, E-W and N-S directions. The

NW-SE trend is strongly developed than the other identified trends. It could represent the prevailing tectonic trend in the area, and it could have played an important role in the formation of its tectonic framework.

In summary, there is: 1) a family of E-W, N-S, NE-SW and NW-SE structural features, which corresponds to contacts associated to several deep-buried faults (F1, F6, F8 and F9); and 2) circular structures interpreted as circular contacts (C1 to C4) or delineation of intrusive bodies (I).

4.5. The Euler Method

In this work, to enhance the estimation of the depth to basement solutions, the 3D Euler Deconvolution technique was performed on the Bouguer data in an attempt to find depth to basement of lineaments. The procedure is realised with a window size of 10 grid cells, a depth tolerance of 15% and, structural indices 0 and 0.5 to efficiently locate contact boundaries, faults and dykes. These structural index values are commonly used in gravity studies for that purposes [21] [43]-[47].

Figure 9 and Figure 10 below show the results of the Euler method applied to the

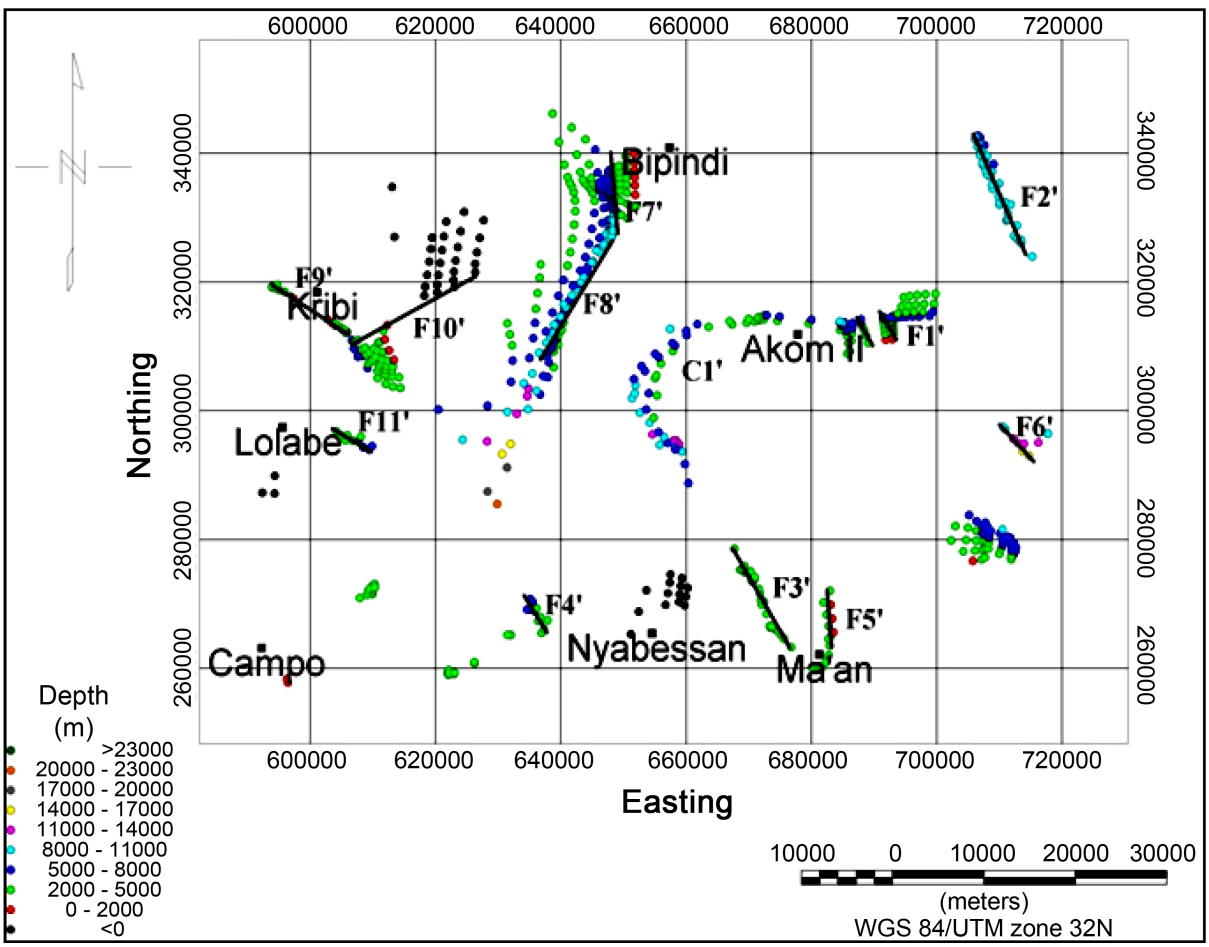

Figure 9. Euler solutions map for a structural index N = 0, with a window size of 10 grid cells, a depth tolerance of 15%. The different black lines represent the outlining lineaments.

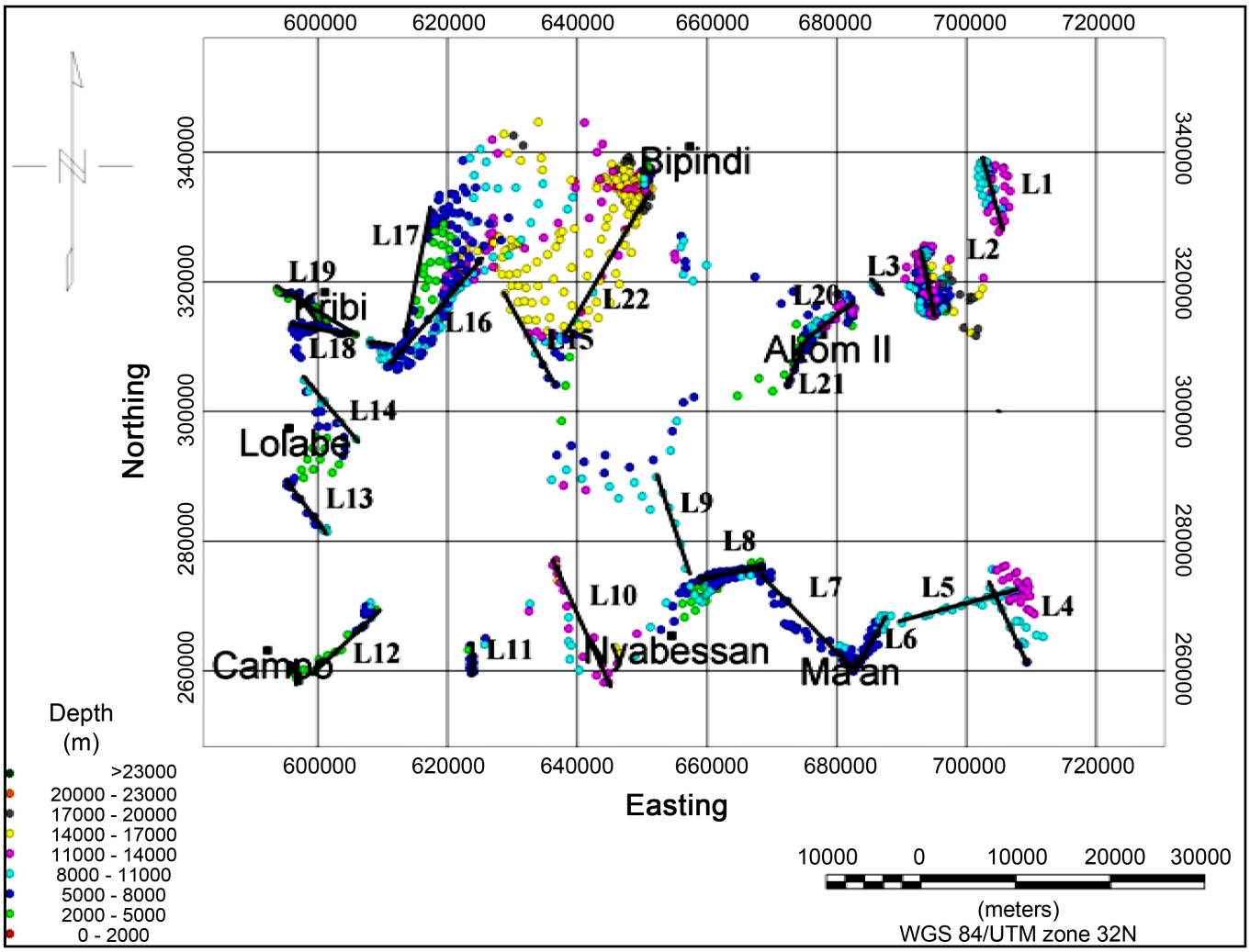

Figure 10. Euler solutions map for a structural index N = 0.5 with a window size of 10 grid cells, a depth tolerance of 15%. The black lines represent the highlighted lineaments.

Bouguer map (Figure 3) for the SI value of 0. The structural interpretation map of the area (Figure 9) shows the different features affecting the area. The computational results reveal that the depths obtained range between 2 and more than 16 km. Outputs from the technique show that there are many linear segments trending in NW, NNW and N-S directions. While linear elements correspond to faults or basement fractures, curved elements express the presence of a probable deep contacts or geological boundaries. Most of these lineaments (interpreted as F1', F2' and F9' faults) trends are consistent with some previous directions highlighted by the maxima of the horizontal gradient magnitude. The recorded depths (up to the [8 km - 11 km] interval) show they could be considered as buried faults. In addition, Euler solutions show non-uniform depth distribution.

Euler solutions for the structural index 0.5 (Figure 10) also show good clustering along the linear and circular segments which trend in the NW, NNW, NNE, E-W and N-S directions. There are many new structural features/ lineaments highlighted (Figure

10). The depth estimates range from 2 km to 21 km for the subsurface structures.

Comparison of the two Euler Deconvolution solutions maps (**Figure 9** and **Figure 10**) enhances the delineation of most structural features. Lineaments L1 and L2 line up in the same direction as F2' and F1', while L7, L19 and L22 are superimposed on F3', F9' and F8' faults. These significant facts exhibit the real location and extension of these vertical-dipping features (L7 and L19, as well) which trend NW, NNE and N-S.

5. Discussion

The obtained Bouguer anomaly map (**Figure 3**) from the study area displays three main types of gravity anomalies over the study area: high, intermediate and low. The general disposition of anomalies on the Bouguer map (**Figure 3**) shows a west-to-east decrease in the anomaly field values associated to a same trending decrease in density. It indicates that the formations to the west are denser than those to the east, as we move from the shore to the hinterland. The anomaly peak at Ma'an is affected by a NE discontinuity that can be interpreted as a lineament. Accordingly with [10], this approximately NE discontinuity could be related to the existence of important NNE fault direction into which tectonic movements or geodynamic evolution would have been developed during different geological ages. In accordance with the results of [1] and [48], it has been found that this regional field stress is in agreement with Eburnean orogeny trend. The same observation of the Bouguer gravity map tends to suggest the existence of NE-SW discontinuity between Akom II and Nyabessan. This is probably a shear zone or fault affecting the deep basement. The faulting that affects the deep basement herein is in accordance with results from [11] and [49] which confirmed the CC/NEFB collision and highlighted NE-SW and NW-SE lineaments in the basement, in an adjacent and more extended area east of the current study area. The gravity anomaly field herein may correspond to the signature of the Archaean basement of the study area. The intermediate gravity anomaly field domain narrows to the north at the vicinity of Bipindi and it is separated to the east by a NW-SE trending domain (herein referred to as the NE domain) of very low gravity values. As can be observed, the corresponding gravity anomalies correlate fairly well with the geology. In particular, the gravity lows fairly delimit the basin. The gravity data analysis enabled to highlight many NNE-SSW to N-S fractures and faults which are local relays of the Kribi-Campo Fault related to the Kribi Shear Zone, also recognized in [2] as the southern extend of the Eseka-Dja fault-line highlighted by [50].

In this study, the results (locations and depths) obtained from the analytical method were compared. The deep-seated structures, interpreted from different maps, are displayed in black lines. The horizontal gradient magnitude peaks were interpreted in two ways. The first interpretation correlates their arrangement with the edge of intrusive rocks, while the second correlates it with faults and fractures. Analysis of the whole map (**Figure 7**) highlights the existence of: 1) contacts and faults trending E-W, N-S, NE-SW and NW-SE, which are either deep and/or buried structures (F1, F6, F8 and F9); and 2) the circular features which may correspond to contacts (C1 to C4) or intrusive bodies (I). The E-W, N-S, NE-SW and NW-SE faults herein highlighted are in ac-

cordance with those resulting from some aeromagnetic investigations over the Southern Cameroon by [51] and [52], east of study area.

The 3-D Euler Deconvolution analysis clearly exhibits NW, NNW and N-S lineaments (either faults or contacts). The Euler's solution plots show non-uniform depth distribution, with estimates ranged from 2 km to 21 km which are in good correlation with the depth range obtained by [1]. Generally, Euler solutions for structural index values retained show good clustering along the NW, NNW, NNE, E-W and N-S directions, though the NW-SE trend is more developed than the other trends. This could represent a past prevailing tectonic trend in the study area. The study assumes this trend seems to correspond to a relay of the faulting related to the Equatorial Atlantic opening, in accordance with [18].

The faults acknowledge the brittle tectonics that affects the Archean to Paleoproterozoic basement of the study area (which belongs to the Congo Craton). These were reactivated by neo and post Proterozoic activities. While the post Proterozoic NNE-SSW to N-S trends are correlated to the South Atlantic Ocean opening, in accordance with previous studies over southwest Cameroon. The present study argues that the NW-SE to E-W oriented structures also correlate with the opening of the Equatorial Atlantic Ocean. This is particularly strengthened by the fact that SW Cameroon seats on a triple junction defined by the West and Central Africa rifts systems.

6. Conclusion

The study investigated the structural features of the Kribi-Campo-Ma'an area in southwestern Cameroon by using the gravity method. The gravity dataset consists of a combination of both historic and new gravity measurements (collected in 2015). The study aims at improving the geological information in the area. The gravity data analysis enables to highlight many NNE-SSW to N-S fractures and faults which are local relays of the Kribi-Campo Fault related to the Kribi shear zone. The faults acknowledge the brittle tectonics that affects the Archean to Paleoproterozoic basement belonging to the Ntem Complex. These faults were reactivated by neo and post Proterozoic activities [11] [12] [49] [51] [52]. While the post Proterozoic NNE-SSW to N-S trends are correlated to the South Atlantic Ocean opening, in accordance with previous studies over south-west Cameroon, the present study argues that the NW-SE to E-W oriented structures also correlate with old faults reactivated during the opening of the Equatorial Atlantic Ocean [18]. In other words, though general believes relate post Panafrican tectonics in the area mainly to the break-up of the Congo-Sao Francisco craton, the break-up of the West Africa-South America should also be considered to affect the area. This is particularly strengthened by the fact that SW Cameroon, and the Kribi-Campo-Ma'an particularly, seats at the vicinity of a triple junction defined by the West and Central Africa rifts systems which affect the whole African plate.

Acknowledgements

The authors are grateful to the reviewers whose remarks and critics would certainly

contribute to the amelioration of the quality of this paper.

References

[1] Owona Angue, M.L.C., Tabod, C.T., Nguiya, S., Kenfack, J.V. and TokamKamga, A.P. (2013) Delineation of Lineaments in South Cameroon (Central Africa) Using Gravity Data. *Open Journal of Geology*, **3**, 331-339. http://dx.doi.org/10.4236/ojg.2013.35038

[2] Owona Angue, M.L.C., Nguiya, S., Nouayou, R., TokamKamga, A.P. and Manguelle-Dicoum, E. (2011) Geophysical Investigation of the Transition Zone between the Congo Craton and the Kribi-Campo Sedimentary Basin (South-West Cameroon). *South African Journal of Geology*, **114**, 145-158. http://dx.doi.org/10.2113/gssajg.114.2.145

[3] Tadjou, J.M., Nouayou, R., Kamguia, J., Kande, H.L. and Manguelle-Dicoum, E. (2009) Gravityanalysis of the Boundary between the Congo Craton and the Pan-African Belt of Cameroon. *Austrian Journal of Earth Sciences*, **102**, 71-79.

[4] Ngako, V., Njonfang, E., Aka, F.T., Affaton, P. and Nnange, J.M. (2006) The North-South Paleozoic to Quaternary Trend of Alkaline Magmatism from Niger-Nigeria to Cameroon: Complex Interaction between Hotspots and Precambrian Faults. *Journal or African Earth Sciences*, **45**, 241-256. http://dx.doi.org/10.1016/j.jafrearsci.2006.03.003

[5] Nzenti, J.P., Barbey, P., Macaudiere, J. and Soba, D. (1988) Origin and Evolution of Late Precambrian High-Grade Yaoundé Gneisses. *Precambrian Research*, **38**, 91-109. http://dx.doi.org/10.1016/0301-9268(88)90086-1

[6] Maurizot, P., Abessolo, A., Feybesse, J.L., Johan, V. and Lecomte, P. (1986) Etude et prospection minière du sud-ouest Cameroun. Synthèse des travaux de 1978 à 1985. Rapport, BRGM, 274 p.

[7] Tadjou, J.M., Manguelle-Dicoum, E., Nguiya, S. and Kamguia, J. (2008) Caractéristiques des anomalies gravimétriques du sous-bassin sédimentaire de Kribi-Campo (Sud-Cameroun). *Africa Geoscience Review*, **1-2**, 39-50.

[8] OwonaAngue, M.L.C. (2012) Investigation géophysique de la zone de transition entre le sous-bassin Sédimentaire de Kribi-Campo et la bordure nord-ouest du Craton du Congo. Doctorat PhD Thèse, Université de Yaoundé I, Yaoundé, 120 p.

[9] Koumetio, F., Njomo, D., Tatchum, C.N., Tokam, K.A.P., Tabod, C.T. and Manguelle-Dicoum, E. (2014) Interpretation of Gravity Anomalies by Multi-Scale Evaluation of Maxima of Gradients and 3D Modelling in Bipindi Region (South-West Cameroon). *International Journal of Geosciences*, **5**, 1415-1425. http://dx.doi.org/10.4236/ijg.2014.512115

[10] Koumetio, F., Manguelle-Dicoum, E., Ndougsa M.T. and Tabod, C.T. (2001) Gravity Study of the Faulting Tectonics around the Western Frontier of the Congo Craton in the Kribi Region (Cameroon). *Journal de la Société Géosciences du Cameroun*, **1**, 62-63.

[11] Shandini, Y.N., Tadjou, J.M., Tabod, C.T. and Fairhead, J.D. (2010) Gravity Data Interpretation in the Northern Edge of the Congo Craton, South-Cameroon. *Anuário do Instituto de Geociências*, **33**, 73-82.

[12] Shandini, Y. and Tadjou, J.M. (2012) Interpreting Gravity Anomaly in South Cameroon, Central Africa. *Earth Sciences Research Journal*, **16**, 5-9.

[13] Minyem, D. and Nedelec, A. (1990) Origin and Evolution of the Eseka Gneisses (Cameroon) Archean TTG Reworked in the Panafrican Mobile Belt. 15*th Colloquium of African Geology*, **2**, 21-24.

[14] Ngoumou, P.C., Ndougsa Mbarga, T., Assembe, S.P. and Kofane, T.C. (2014) Evidence of Iron Mineralization Channels in the Messondo Area (Centre Cameroon) Using Geoelectrical (DC & IP) Methods: A Case Study. *International Journal of Geosciences*, **5**, 346-361.

http://dx.doi.org/10.4236/ijg.2014.53034

[15] Tchameni, R., Mezger, K., Nsifa, E.N. and Pouclet, A. (2001) Crustal Origin of Early Proterozoic Syenites in the Congo Craton (Ntem Complex), South Cameroon. *Lithos*, **57**, 23-42. http://dx.doi.org/10.1016/S0024-4937(00)00072-4

[16] Rosendahl, B.R. and Groschel-Becker, H. (1999) Deep Seismic Structure of the Continental Margin in the Gulf of Guinea: A Summary Report. In: Cameron, N.R., Bate, R.H. and Clure, V.S., Eds., *The Oil and Gas Habitats of the South Atlantic*, The Geological Society, London, 75-83. http://dx.doi.org/10.1144/gsl.sp.1999.153.01.05

[17] Burke, K. (1969) Seismic Areas of the Guinea Coast Where Atlantic Fracture Zone Reach Africa. *Nature*, **222**, 655-657. http://dx.doi.org/10.1038/222655b0

[18] Perez-Diaz, L. and Eagles, G. (2014) Constraining South Atlantic Growth with Seafloor Spreading Data. *Tectonics*, **33**, 1848-1873. http://dx.doi.org/10.1002/2014TC003644

[19] Nsifa, E.N. (2005) Magmatisme et évolution géodynamique de l'Archéen au Protérozoïque de la bordure nord-ouest du craton du Congo (complexe du Ntem) au Sud-Ouest Cameroun. Doctoratd'Etat Thèse, Université de Yaoundé I, Yaoundé, 248 p.

[20] Collignon, F. (1968) Gravimétrie et Reconnaissance de la Ré- publique Fédérale du Cameroun. ORSTOM, Paris, 35.

[21] Fairhead, J.D. andOkereke, C.S. (1988) Depths to Major Density Contrasts beneath the West-African Rift System in Nigeria and Cameroon Based on the Spectral Analysis of Gravity Data. *Journal of African Earth Sciences*, **7**, 769-777. http://dx.doi.org/10.1016/0899-5362(88)90018-8

[22] Anderson, E.D. (2013) Aeromagnetic Signatures of the Geology in Mineral Resources near the Pebble Porphyric Cu-Au-Mo Deposit, Southwest Alaska. PhD Thesis, Colorado School of Mines, Golden, 112.

[23] Biyiha-Kelaba, W., Ndougsa-Mbarga, T., Yene-Atangana, J.Q., Ngoumou, P.C. and Tabod, C.T. (2013) 2.5D Models Derived from the Magnetic Anomalies Obtained by Upwards Continuation in the Mimbi Area, Southern Cameroon. *Journal of Earth Sciences and Geotechnical Engineering*, **3**, 175-199.

[24] Teskey, D.J. and Hood, P.J. (1991) The Canadian aeromagnetic Database: Evolution and Applications to the Definition of Major Crustal Boundaries. *Tectonophysics*, **192**, 41-51. http://dx.doi.org/10.1016/0040-1951(91)90245-N

[25] Grant, F.S. and West, G.F. (1965) Interpretation Theory in Applied Geophysics. McGraw-Hill Book Co., New York, 583 p.

[26] Reeves, C. (2005) Aeromagnetic Surveys: Principles, Practice and Interpretation. Earthworks, Washington DC, 155 p.

[27] Blakely, R.J. (1996) Potential Theory Applied in Gravity and Magnetic Application. Reprinted Edition, Cambridge University Press, Cambridge, 441 p.

[28] Milligan, P.R. and Gunn, P.J. (1997) Enhancement and Presentation of Airborne Geophysical Data. *Journal of Australian Geology & Geophysics*, **17**, 63-75.

[29] Cordell, L. and Grauch, V.J.S. (1985) Mapping Basement Magnetization Zones from Aeromagnetic Data in the San Juan Basin, New Mexico. In: Hinze, W.J., Ed., *The Utility of Regional Gravity and Magnetic Anomaly Maps*, Society of Exploration Geophysicists, 181-197. http://dx.doi.org/10.1190/1.0931830346.ch16

[30] Noutchogwe, T.C., Koumetio, F. and Manguelle-Dicoum, E. (2010) Structural Features of South-Adamawa (Cameroon) Inferred from Magnetic Anomalies: Hydrogeological Implications. *Comptes Rendus Geoscience*, **342**, 467-474. http://dx.doi.org/10.1016/j.crte.2010.03.004

[31] Mohammad, A. (2014) Estimating the Hidden Gravity Lineaments Depths by Using Special Function Method and Comparing Them with the Earthquake Focal Depths: A Case Study of Gujarat Province. *Geodynamics Research International Bulletin*, 56-62.

[32] Phillips, J.D. (2000) Locating Magnetic Contacts: A Comparison of the Horizontal Gradient, Analytic Signal, and Local Wavenumber Methods. Society of Exploration Geophysicists, Abstracts with Programs, Calagry.

[33] Blakely, R.J. and Simpson, R.W. (1986) Approximating Edges of Source Bodies from Magnetic or Gravity Anomalies. *Geophysics*, **51**, 1494-1498. http://dx.doi.org/10.1190/1.1442197

[34] Saad, B. and Taoufik, M. (2006) Horizontal Gradient Signature of Morocco Bouguer Anomaly. *Theoria*, **15**, 25-31.

[35] Thompson, D.T. (1982) EULDPH—A New Technique for Making Computer Assisted Depth Estimates from Magnetic Data. *Geophysics*, **47**, 31-37. http://dx.doi.org/10.1190/1.1441278

[36] Reid, A.B., Allsop, J.M., Granser, H., Millet, A.J. and Somerton, I.W. (1990) Magnetic Interpretation in Three Dimensions Using Euler Deconvolution. *Geophysics*, **55**, 80-91. http://dx.doi.org/10.1190/1.1442774

[37] Reid, A.B. and Fitzgerald, D.J. (2005) Hybrid Euler Magnetic Basement Depth Estimation: Bishop 3D Tests. In: *SEG Technical Program Expanded Abstracts*, 671-674. http://dx.doi.org/10.1190/1.2144412

[38] Foulger, G.R. and Pierce, C. (2007) Geophysical Methods in Geology. Teaching Handbook, University of Durham, Durham, 78 p.

[39] Cordell, L. (1979) Gravimetric Expression of Graben Faulting in Santa Fe Country and the Espanola Basin, New Mexico. In: Ingersoll, R.V., Ed., *Guidebook to Santa Fe Country*, New Mexico Geological Society, Socorro, 59-64.

[40] Archibald, N.J., Gow, P. and Boschetti, F. (1999) Multiscale Edge Analysis of Potential Field Data Exploration. *Geophysics*, **30**, 38-44.

[41] Murphy, F.C. (2008) Architecture: Worms and What They Can Show. New Perspectives: The Foundations and Future of Australian Exploration. *Pmd* CRC Conference*, Geoscience Australia Record, Perth, 11-12 June 2008, 45-51.

[42] Holden, D., Archibald, N., Boschetti, F. and Jessell, M. (2001) Inferring Geological Structures Using Wavelet-Based Multiscale Edge Analysis and Forward Models. *Exploration Geophysics*, **31**, 617-621. http://dx.doi.org/10.1071/EG00617

[43] Reid, A.B. (2003) Short Note: Euler Magnetic Structural Index of a Thin Bed Fault. Geophysics, **68**, 1255-1256. http://dx.doi.org/10.1190/1.1598117

[44] Silva, J.B.C. and Barbosa, V.C.F. (2003) Euler Deconvolution: Theoretical Basis for Automatically Selecting Good Solutions. *Geophysics*, **68**, 1962-1968. http://dx.doi.org/10.1190/1.1635050

[45] Stavrev, P.Y. (1997) Euler Deconvolution Using Differential Similarity Transformations of Gravity or Magnetic Anomalies. *Geophysical Prospecting*, **45**, 207-246. http://dx.doi.org/10.1046/j.1365-2478.1997.00331.x

[46] Marson, I. and Klingele, E.E. (1993) Advantages of Using the Vertical Gradient of Gravity for 3-D Interpretation. *Geophysics*, **58**, 1588-1595. http://dx.doi.org/10.1190/1.1443374

[47] Fairhead, J.D., Bennet, K.J., Gordon, D.R.H. and Huang, D. (1994) Euler: Beyond the "Black Box". In: *SEG Technical Program Expanded Abstracts*, 422-424. http://dx.doi.org/10.1190/1.1932113

[48] Boukeke, D.B. (1994) Structures Crustales d'Afrique Centrale Déduites des Anomalies Gravimétriques et Magnétiques: Le Domaine Précambrien de la République Centrafricaine et du Sud Cameroun. PhD Thesis, Université de Paris Sud, Paris, 263 p.

[49] Basseka, C.A., Shandini, Y. and Tadjou, J.M. (2011) Subsurface Structural Mapping Using Gravity Data of the Northern Edge of the Congo Craton, South Cameroon. *Geofizika*, **28**, 229-245.

[50] Manguelle-Dicoum, E., Bokossah, A.S. and Kwende-Mbanwi, T.E. (1992) Geophysical Evidence for a Major Precambrian Schist-Granite Boundary in Southern Cameroon. *Tectonophysics*, **205**, 437-446. http://dx.doi.org/10.1016/0040-1951(92)90447-E

[51] FeumoeSiyapdje, A.N., NdougsaMbarga, T., Manguelle-Dicoum, E. and Fairhead, J.D. (2012) Delineation of Tectonic Lineaments Using Aeromagnetic Data for the South-East Cameroon Area. *Geofizika*, **29**, 175-192.

[52] Ndougsa-Mbarga, T., FeumoeSiyapdje, A.N., Manguelle-Dicoum, E. and Fairhead, J.D. (2012) Aeromagnetic Data Interpretation to Locate Buried Faults in South-East Cameroon. *Geophysica*, **48**, 49-63.